

PCCP

Accepted Manuscript



This is an *Accepted Manuscript*, which has been through the Royal Society of Chemistry peer review process and has been accepted for publication.

Accepted Manuscripts are published online shortly after acceptance, before technical editing, formatting and proof reading. Using this free service, authors can make their results available to the community, in citable form, before we publish the edited article. We will replace this *Accepted Manuscript* with the edited and formatted *Advance Article* as soon as it is available.

You can find more information about *Accepted Manuscripts* in the [Information for Authors](#).

Please note that technical editing may introduce minor changes to the text and/or graphics, which may alter content. The journal's standard [Terms & Conditions](#) and the [Ethical guidelines](#) still apply. In no event shall the Royal Society of Chemistry be held responsible for any errors or omissions in this *Accepted Manuscript* or any consequences arising from the use of any information it contains.

Cite this: DOI: 10.1039/c0xx00000x

www.rsc.org/xxxxxx

ARTICLE TYPE

Photocatalytic reduction of *o*-chloronitrobenzene under visible light irradiation over CdS quantum dot sensitized TiO₂

Pingjing Chang,^{a,b,c} Haiyang Cheng,^{*a,b} Wei Li,^{a,b} Linhai Zhuo,^{a,b} Limin He,^{a,b,c} Yancun Yu^{a,b} and Fengyu Zhao^{*a,b}

5 Received (in XXX, XXX) Xth XXXXXXXXX 20XX, Accepted Xth XXXXXXXXX 20XX
DOI: 10.1039/b000000x

The photocatalytic activity of the hybrid catalysts of CdS/P25 was studied under visible-light irradiation. The CdS quantum dots sensitized P25 (CdS QDs-P25) showed extremely enhanced activity in the reduction of *o*-chloronitrobenzene (*o*-CNB) by comparing to CdS-P25 prepared by the direct deposition-precipitation method in the presence of HCOOH. The synergistic effects between CdS QDs and P25 could benefit the separation of photogenerated carriers in space and thus the combination of photoelectrons and holes was prevented, and the CdS QDs could provide more photocharges than CdS due to the particle size effect. Furthermore, the process of the photocatalytic reduction in present system was investigated, under the irradiation of visible-light, the photogenerated electrons transferred from the valence band (VB) to the conduction band (CB) of CdS QDs, and injected into the CB of inactivated P25. Meanwhile, the holes generated in the VB of CdS QDs could oxidize HCOO⁻ to give •CO₂⁻ and H⁺. Then, *o*-CNB was reduced to *o*-chloroaniline (*o*-CAN) by the couple of e⁻ and •CO₂⁻ with H⁺. It is a significant method and green process for hydrogenation of nitrocompounds, which may have a great potential application in the reduction of various organic chemicals.

20 1. Introduction

Photocatalysis has received increasing interests owing to its potential applications in organic synthesis reaction,¹⁻³ environmental cleaning^{4,5} and H₂ energy generation.⁶⁻⁹ TiO₂-based materials are one kind of the most extensively studied semiconductors for photocatalysis due to their strong oxidizing ability, high stability, low cost and nontoxicity.¹⁰ However, they can be only activated by ultraviolet (UV) lights due to the large energy bandgap (E_g=3.2 eV), which accounts for less than 5% of sunlight and limits their practical applications. Moreover, the rapid recombination of photogenerated electrons and holes will lead to the low photocatalytic activity of TiO₂. Some methods have been explored to overcome these drawbacks, one of which is coupling TiO₂ with semiconductor, which has more narrow band gap and higher CB, such as CdS,¹¹ Cu₂O,¹² Bi₂WO₆,¹³ ZnFe₂O₄,¹⁴ AgIn₅S₈¹⁵ and Ag₃PO₄.¹⁶ CdS is the most studied one due to its relatively high absorption coefficient in the visible light region except for the narrow band gap (E_g=2.42 eV) and the high CB.¹⁷ In the CdS/TiO₂ composite, visible light can be harvested by the narrow-band gap semiconducting CdS component, while the photogenerated electrons in CdS migrate into the CB of TiO₂. Such a charge-transfer process leads to a spatial separation of the photogenerated electrons and holes and a decrease of their recombination rate. Thus, the photocatalytic efficiency is enhanced. The CdS/TiO₂ composites in various morphologies have been prepared via different synthetic routes.¹⁸⁻³² From the

standpoint of synthesis, the hybridization of TiO₂ with CdS is mainly achieved by the deposition of CdS nanoparticles to the surface of anatase- or rutile-structured TiO₂ microcrystal.^{33,34} Such a surface sensitization is not so effective in transferring electrons between CdS and TiO₂, because of the limited contact of them. Thus, it is necessary to explore the hybrid material of CdS-TiO₂ with stronger contact. The cadmium sulfide quantum dots (CdS QDs) have size-dependent bandgaps and high cross sections for multiphoton absorption,^{35,36} which can yield multiple electron-hole pairs following the absorption of a single photon under certain conditions.^{37,38} To intimately attach CdS QDs to TiO₂, one effective route is linker-assisted assembly by bifunctional molecules.^{21,39-42} Linker-assisted assembly may afford greater control over the size and the electronic properties of the adsorbed QDs, and control over the distance and the electronic coupling between QDs and TiO₂.^{43,44} It was reported that mercaptopropionic acid was used as bifunctional linker to couple CdS QDs with the mesoporous TiO₂, and the formed CdS QDs-TiO₂ with the linking molecule of mercaptopropionic acid exhibited higher stability and activity than CdS-TiO₂ prepared by direct deposition.⁴⁵ Moreover, CdS-trititanate nanotube composite material with the linking molecule of mercaptopropionic acid was reported to be effective for the visible light-induced photocatalytic water splitting.⁴⁶ Catalytic hydrogenation is one of the most important reactions, in which autoclaves and the handling of hydrogen is generally required. By comparison, the transfer hydrogenation with hydrogen source such as formic acid, formate, hydrazine, and

sodium borohydride provides an attractive alternative. Very recently, increasing attention has been paid to the photocatalytic reduction of organic compounds,⁴⁷⁻⁵³ Kominami et al. reported that TiO₂ was an active photocatalyst for the photoreduction of nitroarenes to aminearenes in aqueous solution in the presence of hole scavengers under UV irradiation.⁴⁷ Wu et al. reported that microcrystalline SrBi₂Nb₂O₉ and nanocrystalline PbBi₂Nb₂O₉ were efficient catalysts for the photoreduction of *p*-nitroaniline to *p*-phenylenediamine in aqueous suspension under UV and visible light irradiation.^{48,54} They also studied the photoreduction of *p*-nitroaniline over TiO₂, ZnO, PbBi₂Nb₂O₉ and CdS in the presence of CH₃OH, C₂H₅OH and *i*-C₃H₇OH.⁴⁹ However, the photocatalytic mechanism is still not clear, and the photocatalytic activity needs further to be improved.

To enhance the photocatalytic activity, CdS QDs were intimately tethered to the surface of TiO₂ by using L-cysteine, in which thiol and amino groups were binded strongly to the surface of CdS QDs and the carboxyl group was firmly binded to the surface of TiO₂, forming CdS QDs-TiO₂ with stronger contact. For comparison, CdS-TiO₂ was also prepared by the direct deposition-precipitation method. The photocatalytic activity of the above catalysts was studied in the reduction of *o*-chloronitrobenzene (*o*-CNB) under the visible light irradiation. Moreover, the mechanism of the photoreduction over CdS QDs-TiO₂ was proposed.

2. Materials and methods

2.1. Material Preparation

P25 was purchased from Acros Organics and used as received. Ethanol, NaOH, CdCl₂•2.5H₂O, Na₂S•9H₂O, L-cysteine, (COOH)₂, HCOOH, HCOOK, HCOONa, HCOONH₄ and *o*-CNB from Beijing Chemical Reagent Cooperation, are of analytical grade and used without further purification. Gas of N₂ (99.999%) and H₂ (99.999%) (Changchun Xinxing Gas Company) was used as delivered.

In a typical preparation, 27.3% CdS QDs-P25 was synthesized as follows: 0.68 g L-cysteine was dissolved into 30 ml deionized water with stirring. Then 0.24 g P25 was dispersed in the above solution under vigorous stirring. CdCl₂ (0.34 g) aqueous solution (6 ml) was then added. Thereafter, the pH value was tuned to 12.5 with 1 M NaOH solution and Na₂S (0.19 g) aqueous solution (15 ml) was slowly added. The solution was refluxed at 383 K for 5 h. The resulting composite was centrifugated and washed with distilled water, and dried at 353 K for 12 h. As determined by ICP, The content of CdS (mass ratio) in the CdS QDs-P25 was denoted as *x*%, and four samples with *x*=15.7, 19.6, 27.3, 31.7 were prepared. Pristine CdS QDs was also synthesized following the same procedure as mentioned above without the addition of P25.

CdS-P25 was prepared by a deposition-precipitation method.⁵⁵ In a typical preparation, CdCl₂•2.5H₂O (0.46 g) was added to 30 ml ethanol. After the cadmium salt dissolved completely, P25 (0.67 g) was added, and the solution was stirred vigorously at 343 K, a Na₂S (2.30 g) aqueous solution (80 ml) was then dropwise added. After stirring for 7 h, the resulting composite was centrifugated and washed with distilled water, and dried at 353 K for 12 h. As determined by ICP, four samples with *x*%=15.0%,

30.0%, 47.5%, 61.2% were prepared. Pristine CdS was also synthesized following the same procedure as mentioned above without the addition of P25.

2.2. Characterization

Powder X-ray diffraction (XRD) was performed using a Bruker D8 Advance X-ray diffract meter with a Cu K α source at 40 kV and 40 mA. 2 θ scans were performed from 10° to 90° at a 4°/min speed. Transmission electron microscopy (TEM) was carried out in a JEOL JEM-2010 instrument operating at an accelerating voltage of 200 kV. The TEM samples were prepared by dispersing the catalyst powder in ethanol under ultrasonic for 5–10 min and then the resulted solution was dropped on a carbon film of copper grid. Fourier transform infrared spectra (FT-IR) were measured on a Vertex Perkin-Elmer 580BIR spectrophotometer (Bruker) with the KBr pellet technique. X-ray photoelectron spectroscopy (XPS, VG Microtech 3000 Multilab) was used to examine the electronic properties of the photocatalysts. The C 1s peak at 284.6 eV arising from adventitious carbon was used as reference. This reference gives binding energy values with a precision of ± 0.2 eV. Diffuse reflectance UV/vis spectra were recorded with a Shimadzu UV-3100 PC spectrophotometer.

¹³C CP MAS spectra were recorded on a Bruker AVANCE III 400 WB spectrometer equipped with a 4 mm standard bore CPMAS probehead whose X channel was tuned to 100.62 MHz for ¹³C and the other channel was tuned to 400.18 MHz for broad band ¹H decoupling, using a magnetic field of 9.39T at 297 K. The dried and finely powdered samples were packed in the ZrO₂ rotor closed with Kel-F cap which were spun at 5 kHz rate. The experiments were conducted at a contact time of 2 ms. A total of 10000 scans were recorded with 3 s recycle delay for each sample. All ¹³C CP MAS chemical shifts are referenced to the resonances of adamantane (C₁₀H₁₆) standard (δ_{CH_2} =38.5).

2.3. Photoelectrochemical Measurement

Working electrodes were prepared as follows: 20 mg of sample was ground with 0.5 ml terpineol. The slurry was then coated onto an indium–tin oxide glass by the doctor blade method. These electrodes were preliminary dried at 80 °C and calcined at 200 °C for 1 h under Ar atmosphere. All investigated electrodes had a similar film thickness. Photocurrents were measured using an electrochemical analyzer (CHI660D Instruments) in a standard three electrode system by using the prepared sample film as the working electrodes (an effective area of 2 cm²), a Pt flake as the counter electrode, and saturated calomel electrode as the reference electrode. Bias potential applied on the working electrode was 0.5 V. A 300 W Xe-lamp (Beijing Trusttech Co. Ltd., China) served as a light source to irradiate the working electrode from the back side. A 0.1 M NaClO₄ solution was used as the electrolyte.

2.4. Photocatalytic Activity Measurement

In a typical photoreduction process, catalyst (20 mg), *o*-CNB (0.25 mmol), HCOOH (1.5 mmol) and H₂O (5 ml) were successively charged into the self-designed quartz reactor. Then, the reactor was sealed and flushed three times with N₂ to remove the air. After flushing, the reactor was heated up to 35 °C. The reaction mixture was stirred in the dark for 20 min to ensure the establishment of adsorption–desorption equilibrium between the

catalyst and *o*-CNB. Then, the photoreduction was initiated by irradiating with one 300 W Xe lamp (CEL-HXUV 300, Beijing CHN EDU AuLight Co.). All the lights with the wavelength less than 420 nm were cut off by an optical filter (UV-CUT 420). The reaction system was stirred vigorously at 1200 rpm to eliminate diffusion limit. After reaction for 2 h, the product was extracted with 5 ml diethyl ether and analyzed with a gas chromatograph (GC-Shimadzu-2010, FID, Capillary column, Rtx-5 30 m × 0.25 mm × 0.25 μm), and identified by gas chromatography/mass spectrometry (GC/MS, Agilent 5890). The conversion and selectivity were calculated using the following equations:

$$\text{Conversion (\%)} = \left(1 - \frac{m_{o\text{-CNB}}}{m_{o\text{-CAN}} + m_{o\text{-CNB}} + m_{\text{by-products}}} \right) \times 100\%$$

$$o\text{-CAN selectivity (\%)} = \frac{m_{o\text{-CAN}}}{m_{o\text{-CAN}} + m_{\text{by-products}}} \times 100\%$$

where $m_{o\text{-CNB}}$, $m_{o\text{-CAN}}$, and $m_{\text{by-products}}$ represent the mole ratio of *o*-CNB, *o*-CAN, and by-products in the mixture, and the carbon balance values calculated from *o*-CNB, *o*-CAN and by-products are around 100%.

The gas products were collected and analyzed with a gas chromatograph using the TCD detector (TDX-01, 2 m) and identified with pure H₂, O₂, CO and CO₂ to confirm the production of H₂ and CO₂ during the reaction. The H₂ or/and CO₂ produced during the reaction has been collected by water removing method with saturated NaHCO₃ and calculated by the ideal gas equation. In the absence of *o*-CNB, the mole ratio of H₂:CO₂ was 1:1, but in the presence of *o*-CNB, only CO₂ was detected.

3. Results and discussion

3.1 Characterization of CdS-P25 and CdS QDs-P25

FT-IR spectroscopy was measured to examine the existence of L-cysteine in the prepared CdS QD-TiO₂ sample with CdS as a reference (Fig. 1a). For pure P25, vibration of Ti-O-Ti bond presented at a low frequency band ca. 447 cm⁻¹ (Fig. 1b). However, the vibration of Ti-O-Ti showed a blue shift for the as-prepared CdS-P25 and CdS QDs-P25 (Fig. 1c, d), and the latter shifted to a much higher wavenumber of 502 cm⁻¹. In fact, the peak at 502 cm⁻¹ could be attributed to the combination of Ti-O-Ti vibration and Ti-O-C vibration of CdS QDs-P25.⁵⁷ The presence of Ti-O-C bonds indicated that L-cysteine interacted with the surface hydroxyl group of P25 through its carboxylic group.⁵⁸ For L-cysteine, the peak at 1393 and 1585 cm⁻¹ corresponded to the asymmetric and symmetric stretching bands of the carboxylate ($\nu_s(\text{CO}_2^-)$ ⁵⁹⁻⁶¹ and $\nu_a(\text{CO}_2^-)$ ⁵⁹⁻⁶³, respectively; the peaks at 1544 and 3174 cm⁻¹ corresponded to the asymmetric and symmetric stretching bands of the protonated amine of $\nu_s(\text{NH}_3^+)$ ^{59,61} and $\nu_a(\text{NH}_3^+)$ ⁶¹, respectively; and the peak at 2552 cm⁻¹ corresponded to the thiol group⁵⁹⁻⁶¹ (Fig. 1g). However, the characteristic peak of the -SH group was not observed in CdS QDs-P25 and CdS QDs, and the asymmetric stretching band of the protonated amine in L-cysteine (3174 cm⁻¹) disappeared, but the broad $\nu(\text{NH}_2)$ band (3200-3500 cm⁻¹) appeared in CdS QDs-P25 and CdS QDs (Fig. 1d, 1f). The peaks at around 1023-1180 cm⁻¹ are mainly due to C-OH stretching of residual ethanol (Fig. 1a) or L-cysteine (Fig. 1f, 1g), and they are weakened in CdS QDs-P25 and L-cysteine/P25 for that L-cysteine interacted with the

surface hydroxyl group of P25 through its carboxylic group. The peaks at 1405 and 1631 cm⁻¹ corresponded to the asymmetric and symmetric stretching bands of the carboxylate ($\nu_s(\text{CO}_2^-)$ and $\nu_a(\text{CO}_2^-)$) in P25 supported L-cysteine (L-cysteine/P25) (Fig. 1e). The coverage of L-cysteine was about 6% in 27.3% CdS QDs-P25 and 8% in L-cysteine/P25 based on the results of TGA (Fig. S1) and ICP measurement. These results indicated that CdS QDs tethered with L-cysteine through thiol group^{59-61,64} and amine group^{59,65,66}. In this way, CdS QDs tethered to TiO₂ intimately through -SH, -NH₂ and -COOH groups of L-cysteine.

Solid state ¹³C NMR spectra of L-cysteine and CdS QDs-P25 are shown in Fig. 2. Two sharp peaks in the spectrum of L-cysteine at $\delta(^{13}\text{C})$ 27.36 and 55.33 ppm were ascribed to C_β (-SH) and C_α (-NH₂),⁶¹ respectively, and these peaks were also found in the spectrum of CdS QDs-P25, which indicated that CdS QDs were successfully tethered to P25 through L-cysteinate. This is in agreement with the above results of FT-IR spectra. However, the peaks of C_β (-SH) and C_α (-NH₂) were broadened and shifted to downfield of 31.61 and 59.81 ppm. The complexation of metal with S and N atom could cause a decrease of electron density of the S and N atom in L-cysteine, and resulted in deshielding effect on the adjacent carbons⁶⁷ and so induced a downfield shift of C_β (-SH) and C_α (-NH₂) in CdS QDs-P25. In addition, for CdS QDs-P25 sample, a shoulder peak at 55 ppm was ascribed to C_α (-NH₂) of L-cysteine for that free -NH₂ existed due to its uncompleted coordination.

The XRD patterns are shown in Fig. 3. The diffraction peaks at about 26.7°, 43.9°, and 52.2° were corresponding to (1 1 1), (2 2

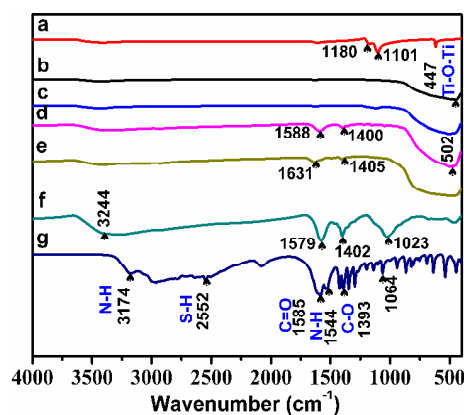


Fig. 1 FT-IR spectra of (a) CdS, (b) P25, (c) 30% CdS-P25, (d) 27.3% CdS QDs-P25, (e) L-cysteine/P25, (f) CdS QDs, and (g) L-cysteine.

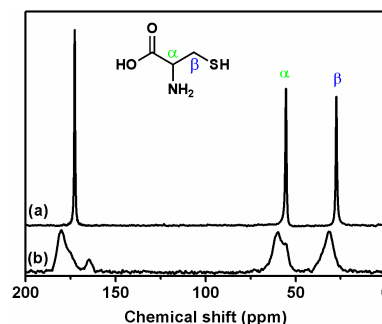


Fig. 2 ¹³C-NMR spectra of (a) L-cysteine and (b) 27.3% CdS QDs-P25.

0), and (3 1 1) of CdS (Fig. 3a-d), respectively, and the cubic CdS was formed as identified by JCPDS 89-0440 file. The bare P25 contained 86% anatase and 14% rutile as estimated by the integral intensities of the anatase (1 0 1) and the rutile (1 1 0) reflections at 25.3° and 27.5° (Fig. 3e). The average crystallite size of bare P25 was approximately 20 nm, estimated from the peak width of anatase (1 0 1) by Scherrer equation. The average crystallite size of CdS was ~6 nm in 27.3% CdS QDs-P25, and ~10 nm in 30% CdS-P25. No significant shifts of principal peaks of CdS, CdS QDs or P25 were observed, which indicates that the crystalline structure of P25 was not influenced by the deposition of CdS or CdS QDs (Fig. 3c, d).

The TEM images of CdS-P25 and CdS QDs-P25 are shown in Fig. 4. The average crystallite size of P25 was ca. 20 nm in these samples (Fig. 4a, c), and it is in agreement with the results of XRD. CdS and TiO₂ were well crystallized, the crystal lattice in 0.20 and 0.35 nm was corresponding to the (2 2 0) facet of cubic crystal CdS and (1 0 1) facet of anatase of TiO₂, respectively (Fig. 4b, d). The particle size of CdS in CdS QDs-P25 (~6 nm) was smaller than that in CdS-P25 (~10 nm). The presence of distinct juncture between two crystal phases could further confirm the strong interaction between CdS QDs and P25 via L-cystine in CdS QDs-P25.

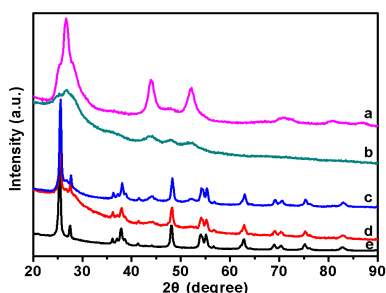


Fig. 3 XRD patterns of (a) CdS, (b) CdS QDs, (c) 30% CdS-P25, (d) 27.3% CdS QDs-P25, and (e) P25.

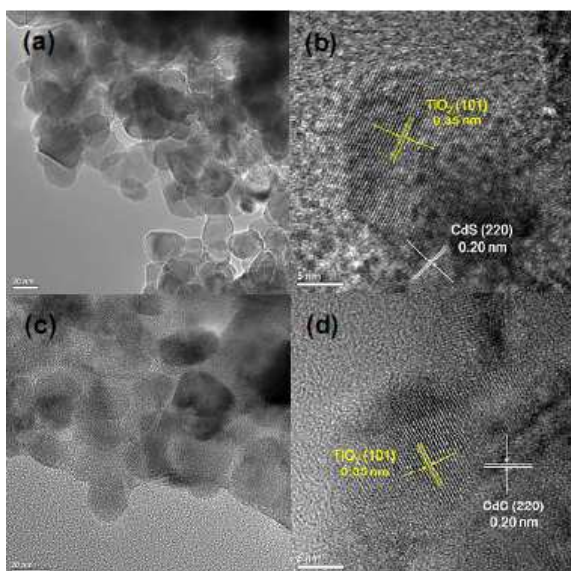


Fig. 4 TEM morphologies of (a, b) 30% CdS-P25 and (c, d) 27.3% CdS QDs-P25.

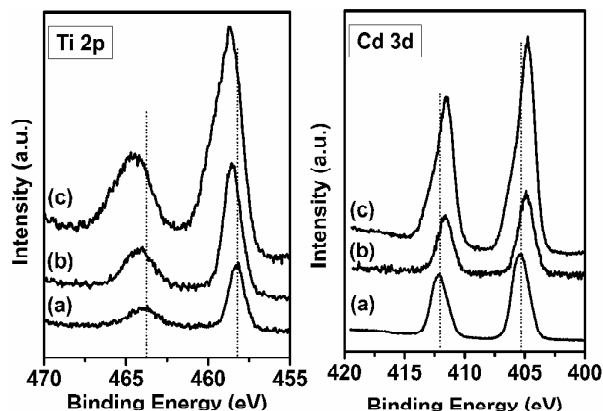


Fig. 5 (Left) XPS spectra of Ti 2p in (a) P25, (b) 30% CdS-P25 and (c) 27.3% CdS QDs-P25, and (right) XPS spectra of Cd 3d in (a) CdS, (b) 30% CdS-P25 and (c) 27.3% CdS QDs-P25.

Fig. 5 shows the XPS spectra of Ti 2p and Cd 3d peaks. The binding energies of Ti 2p_{1/2} and Ti 2p_{3/2} appeared at 464.0 and 458.3 eV for P25. However, they appeared at 464.1 and 458.5 eV for CdS-P25, and 464.4 and 458.8 eV for CdS QDs-P25, respectively. For pure CdS, the binding energies of Cd 3d_{3/2} and Cd 3d_{5/2} appeared at 412.1 and 405.3 eV. However, they appeared at 411.6 and 404.8 eV for CdS-P25, and 411.5 and 404.7 eV for CdS QDs-P25, respectively. The binding energies of Ti 2p in CdS-P25 and CdS QDs-P25 were higher than that in pure P25, meanwhile, the binding energies of Cd 3d in CdS-P25 and CdS QDs-P25 were lower than that in pure CdS, indicating that the electronic density of TiO₂ decreased and that of CdS increased after CdS or CdS QDs attached to P25, indicating that the electron transferred from TiO₂ to CdS. Therefore, an electronic interaction existed between CdS and P25, and it was much stronger in CdS QDs-P25 than that in CdS-P25. The stronger interaction may benefit the transfer of photocharges between CdS QDs and P25 under visible light, thus improving the photocatalytic activity.

3.2 Photocatalytic activity

The photocatalytic activity was examined for the reduction of *o*-CNB under visible light irradiation ($\lambda \geq 420$ nm) in the presence of HCOOH as a sacrificial agent upon purging with N₂. As shown

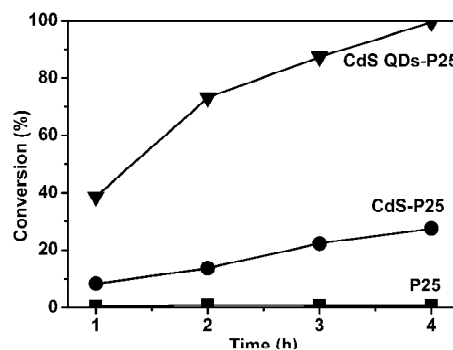


Fig. 6 Photoreduction efficiencies of *o*-CNB as a function of irradiation time over P25 (■), 30% CdS-P25 (●) and 27.3% CdS QDs-P25 (▼). Reaction conditions: 20 mg catalyst, 0.25 mmol *o*-CNB, 1.5 mmol HCOOH, 5 ml H₂O, 35 °C.

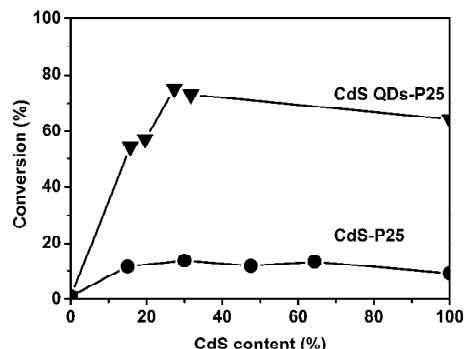


Fig. 7 Photoreduction efficiencies of *o*-CNB over CdS-P25 (●) and CdS QDs-P25 (▼) with increasing of CdS content. Reaction conditions: 20 mg catalyst, 0.25 mmol *o*-CNB, 1.5 mmol HCOOH, 5 ml H₂O, 35 °C, 2 h.

in Fig. 6, the conversion of *o*-CNB was lower than 1.0% over P25 after reaction for 4 h, indicating the activity of P25 is negligible under the visible light region. However, the photocatalytic activity was enhanced obviously and the conversion of *o*-CNB reached to 27.5% over CdS-P25 and 99.5% over CdS QDs-P25 under the same reaction condition.

To investigate the effect of the amount of CdS on the photoreduction efficiency, a series of CdS-P25 and CdS QDs-P25 composites were synthesized with different loading of CdS, and the photocatalytic results are shown in Fig. 7. For CdS-P25, the conversion of *o*-CNB increased from 1.0% to 13.6% with increasing of CdS content to 30%, and then it decreased with further increasing and a 9.1% conversion presented over the pure CdS. Similarly, For CdS QDs-P25, the conversion of *o*-CNB increased from 1.0% to 75.2% with increasing of CdS QDs content to 27.3%, and then it decreased slightly and a 64.4% conversion obtained over CdS QDs. It is obvious that the photocatalytic activity was enhanced largely after coupling TiO₂ with CdS or CdS QDs, and the latter one showed much more improvement.

3.3 The function of CdS QDs

The UV-vis absorption spectrum was examined. As shown in Fig. 8, the absorption edge for pure P25 presented at about 391

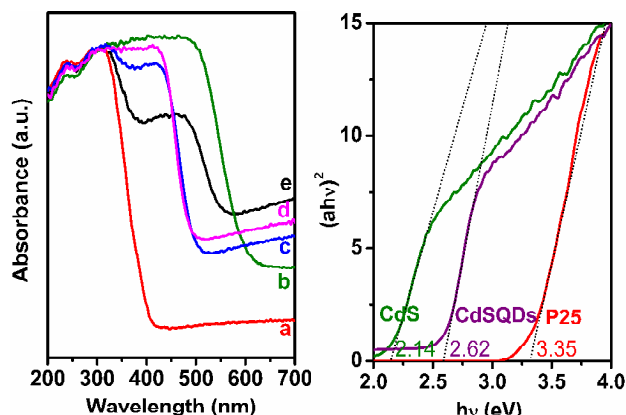


Fig. 8 (Left) the UV-vis absorption spectra of (a) P25, (b) CdS, (c) 27.3% CdS QDs-P25, (d) CdS QDs and (e) 30% CdS-P25, and (right) the Tauc's plot for band gap energy determination.

nm without significant absorption at visible light region (Fig. 8a). However, for CdS and CdS QDs, the absorption edge presented at ca. 597 and 481 nm (Fig. 8b, d), and for 30% CdS-P25 and 27.3% CdS QDs-P25, the absorption edge appeared at ca. 542 and 493 nm (Fig. 8c, e), indicating they are active at the visible region. Compared with CdS QDs, a decrease of bandgap energy was observed in CdS QDs-P25, it was ascribed to the strong electronic coupling between CdS QDs and P25, which make the electron transfer from the VB of CdS QDs to the CB of P25 under visible light irradiation.²¹ The absorption edge of CdS QDs-P25 shifted much more than that of CdS-P25, indicating CdS in the former was much smaller than that in the later one.⁶⁸ So, CdS QDs could provide more photocharges compared with CdS for the particle size effect.

Fig. 9 showed the photocurrent–time (I–t) curves for CdS-P25 and CdS QDs-P25 with typical on–off cycles of intermittent solar irradiation at a bias potential of 0.5 V. As can be seen, the electrode made by CdS QDs-P25 exhibited a superior performance, and its photocurrent generation efficiency was higher than that of CdS-P25. This was ascribed to that the CdS QDs can produce more photocharges than CdS due to the smaller size of CdS QDs and thus it has much more active sites. The stable photocurrent value of CdS QDs-P25 was about 5 times higher than that of CdS-P25. Therefore, the photocatalytic efficiency of CdS QDs-P25 was much higher than that of CdS-P25.

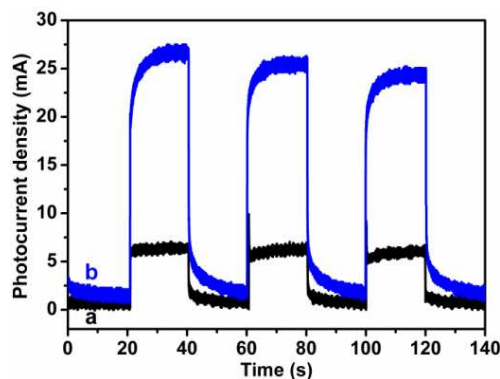


Fig. 9 Transient photocurrent response for (a) 30% CdS-P25 and (b) 27.3% CdS QDs-P25. All the electrodes were evaluated in 0.1 M NaClO₄ aqueous solution under visible light irradiation using a calomel electrode as the reference electrode.

Table 1 values used for the calculation of the conduction and valence band potentials of CdS, CdS QDs and TiO₂

Semiconductor	CE	EA (eV)	IE (eV)	EE (eV)	SE (eV)	E _g (eV)	E _{CB} (eV)	E _{VB} (eV)
CdS	Cd	-0.78	9.01	4.12	5.06	2.14	-0.51	1.63
CdS QDs	S	2.08	10.38	6.23	5.06	2.62	-0.75	1.87
TiO ₂	Ti	0.32	6.12	3.22	5.68	3.35	-0.5	2.85
	O	1.465	13.64	7.55	5.68	3.35	-0.5	2.85

CE: Constituent elements, EA: Electron affinity, IE: Ionization energy, EE: Element electronegativity, SE: Semiconductor electronegativity, E_g: band gap energy, E_{CB}: conduction band edge potential, E_{VB}: valence band edge potential

Table 2 Photoreduction efficiencies of *o*-CNB over CdS-P25 used different sacrificial agent

Entry	Sacrificial agent	Conversion (%)	Selectivity (%)		
			<i>o</i> -CAN	<i>o</i> -CNSB	Others ^a
1	—	—	— ^b	— ^b	— ^b
2	(COOH) ₂	1.4	99.8	0.2	— ^b
3	HCOOH	13.6	95.9	4.1	— ^b
4	HCOOK	16.9	57.2	42.2	0.6
5	HCOONa	18.2	56.7	42.9	0.4
6	HCOONH ₄	25.0	58.3	41.1	0.6

Reaction conditions: 20 mg 30% CdS-TiO₂, 0.25 mmol *o*-CNB, 1.5 mmol sacrificial agent, 5 ml H₂O, 35 °C, 2 h. ^a Intermediates include dichloroazoxybenzene, dichloroazobenzene and dichlorohydroazobenzene. ^b Not detected.

The band edge potentials for the semiconductors were estimated using the equation related to Mulliken electronegativity. Herein, the electronegativity (EE) of an atom was the arithmetic mean of the atomic electron affinity (EA) and the first ionization energy (IE).⁶⁶ The CB potential at the point of zero charge could be calculated according to an empirical equation:⁶⁴

$$E_{CB} = \chi - E^{\circ} - 0.5 E_g$$

where E_{CB} is the CB edge potential, χ is the electronegativity of the semiconductor (SE), which is the geometric mean of the electronegativity of the constituent atoms, E° is the energy of free electrons on the hydrogen scale (about 4.5 eV),¹⁵ E_g is the band gap energy of the semiconductor, which is determined by Tauc's plot in Fig. 8. The VB edge potential (E_{VB}) could be determined by $E_{VB} = E_{CB} + E_g$. The values used to calculate E_{CB} and E_{VB} , and the calculated results of E_{CB} and E_{VB} of CdS, CdS QDs and TiO₂ are listed in Table 1. As can be seen, E_{CB} of CdS (-0.51 eV) was cathodic than that of P25 (-0.5 eV), and also, E_{CB} of CdS QDs (-0.75 eV) was more cathodic than that of P25 (-0.5 eV). In general, the larger the difference between the CBs of the semiconductors, the higher the driving forces of electron injection are,⁶⁹ so CdS QDs-P25 was more efficient than CdS-P25 in photocatalytic reduction of *o*-CNB.

3.4 Mechanism of photocatalysis and the reduction process

The effects of the sacrificial agents on the photoreduction of *o*-CNB to *o*-CAN over CdS-P25 in H₂O were investigated under the visible light irradiation and the results are listed in Table 2. In the absence of sacrificial agent, no significant conversion of *o*-CNB was observed after 2 h (entry 1). When (COOH)₂ was used, a 1.4% conversion was observed (entry 2). When HCOOH was used, the conversion reached to 13.6%, and the selectivity to *o*-CAN was 95.9% (entry 3). When HCOOK, HCOONa, and HCOONH₄ were used, the conversion of *o*-CNB increased, but the selectivity to *o*-CAN dropped significantly, and at last dropped to < 60% (entries 4-6). Evidently, sacrificial agent was indispensable and HCOOH was the most suitable one for the present photocatalytic reaction.

In thermocatalytic reaction, catalytic transfer hydrogenation (TH) was an effective method to reduce organic compounds.^{70,71} However, TH mechanism was still not well understood, in particular for the heterogeneous catalytic TH. Generally, there are two pathways, one is a consecutive dehydrogenation-hydrogenation process, and the other is a true hydrogen transfer

Table 3 Results for the reduction of *o*-CNB under different conditions

Entry	<i>o</i> -CNB (mmol)	HCOOH (mmol)	H ₂ O (ml)	λ (nm)	H ₂ (mmol) ^a	Conv. (%)
1	0.25	1.5	5	— ^b	— ^c	— ^c
2	—	1.5	5	≥ 420	0.02	— ^c
3	0.25	—	5	≥ 420	— ^c	2.2
4 ^d	0.25	—	5	≥ 420	— ^c	2.3
5 ^e	0.25	132.5	—	≥ 420	— ^c	58.6
6	0.25	1.5	5	≥ 420	— ^c	60.0

Reaction conditions: 20 mg 27.3% CdS QDs-P25, 35 °C, 2 h. ^a The amount of H₂ produced. ^b without light irradiation. ^c Not detected. ^d 1 MPa H₂ was introduced during reaction. ^e HCOOH used as solvent and sacrificial agent simultaneously.

process without H₂ molecules. With HCOONa as hydrogen donor, in our previous work, the reduction of citral and phenol over Pd/C proceeded through the consecutive H₂ production-hydrogenation pathway.^{72,73} However, it was reported that the reduction of nitroarenes to aminoarenes was a true hydrogen-transfer process.⁷⁴ What does it occur in the photoreduction? When the sacrificial agents such as CH₃OH, HCOOH were used as hydrogen donors, it may go through a consecutive dehydrogenation-hydrogenation process or a true hydrogen transfer process. In the presence of CH₃OH, C₂H₅OH and *i*-C₃H₇OH, Wu et al. reported that the photoreduction of *p*-nitroaniline to *p*-phenylenediamine over TiO₂ or ZnO was proceeded through the hydrogen transfer reaction between the *p*-nitroaniline and H₂O molecules by the 2H(D)-labeled experiments. However, H₂ was detected in the system,⁴⁹ and the HD exchange was found to occur between D₂O and CH₃OH at the hydroxyl position, thus the photocatalytic mechanism was still not clear.

Herein, to reveal the photoreduction process of *o*-CNB, the reaction was performed under different conditions over CdS QDs-P25 and the results are listed in Table 3. Without light irradiation, the reduction of *o*-CNB could not proceed (entry 1). In the absence of *o*-CNB, 0.02 mmol H₂ was produced. However, in the presence of *o*-CNB, H₂ could not be detected (entry 2, 6). In the absence of HCOOH, the photocatalytic reduction efficiency was low and the conversion of *o*-CNB was < 2.3% whether in the absence or presence of H₂ (entry 3, 4). In the presence of HCOOH, the photocatalytic reduction efficiency was improved dramatically, and similar conversion of *o*-CNB could be obtained with or without H₂O (entry 5, 6). Based on the above results, we can suggest that CdS QDs-P25 could effectively catalyze the reduction of *o*-CNB to *o*-CAN in the presence of HCOOH under visible-light irradiations, the photocatalytic reduction was not induced by the direct hydrogenation with the H₂ generated in situ from HCOOH splitting, but by the hydrogen transfer between HCOOH and *o*-CNB molecules, and the hydrogen was not coming from H₂O but from HCOOH. In addition, in the absence of *o*-CNB, the color of CdS QDs-P25 changed gradually from bright yellow to dark green during the photocatalytic H₂ production. This color change was attributed to the partial reduction of Ti⁴⁺ to Ti³⁺ in the CdS QDs-P25 matrix by the photoexcited electrons. The formed Ti³⁺ cations could not be timely consumed by protons to produce H₂. However, the color of CdS QDs-P25 could be regenerated from dark green to bright

yellow after exposure to air due to that the stored electrons coupled with the protons could be scavenged by O_2 .⁷⁵ It is worth noting that in the presence of *o*-CNB, the color of CdS QDs-P25 did not change during the photocatalytic reduction. In this case, the formed Ti^{3+} cations could couple with the protons to form the positive charge of $Ti-OH^+$ groups (active hydrogen), the active hydrogen was consumed by *o*-CNB as soon as it produced. Therefore, the present reaction is confirmed to be a hydrogen transfer reaction induced by photocatalytic reduction over the CdS QDs-P25 catalyst under the visible light irradiation.

On the basis of the above results, a possible mechanism for the enhanced photoactivity over CdS QDs-P25 was proposed as shown in Fig. 10. The CB of CdS QDs (-0.75 eV) was more cathodic than that of TiO_2 (-0.50 eV). So under visible-light irradiation, once CdS QDs was excited, the photogenerated electrons were excited from VB to CB, and electrons were injected from the CB of CdS QDs into the CB of inactivated TiO_2 . Meanwhile, the VB of CdS QDs (1.87 eV) was more cathodic than that of TiO_2 (2.85 eV), so hole generated in the VB of CdS QDs remained there and could not migrate to TiO_2 . These thermodynamic conditions favored the electron injections. Photoinduced holes could not react with water molecules to give $\bullet OH$ radicals ($h^+ + H_2O \rightarrow \bullet OH + H^+$) due to the low redox potentials of the VB of CdS QDs (EVB (CdS QDs) = 1.87 eV, E ($\bullet OH/H_2O$) = 2.72 eV⁶⁵ vs. SHE). This result further indicated H_2O was not the true hydrogen source in the reaction. HCOOH decomposed to H^+ and $HCOO^-$ in water, and then $HCOO^-$ was oxidized by the photoinduced holes to give $\bullet CO_2^-$ in the VB of CdS QDs ($HCOO^- + h^+ = H^+ + \bullet CO_2^-$), due to the relative high redox potentials of the VB of CdS QDs (EVB (CdS QDs) = 1.87 eV, E ($\bullet CO_2^-/HCOO^-$) = 1.36 eV⁷⁶ vs. SHE). On the other hand, the photogenerated electrons in the CB of CdS QDs migrated and injected to the CB of TiO_2 , which were trapped by Ti^{4+} to form Ti^{3+} cations, and coupled with the protons produced from HCOOH decomposition and $HCOO^-$ oxidization by the photoinduced holes to form the positively charged $Ti-OH^+$ groups, which could be named as the active hydrogen (H^*).^{75,77} The active hydrogen species could instantly and selectively reduce *o*-CNB to *o*-CAN under ambient conditions. Moreover, $\bullet CO_2^-$ oxidized by the photoinduced holes has a strong reducing ability (E ($\bullet CO_2^-/CO_2$) = -1.8 eV⁷⁶ vs. SHE), and can be coupled with the protons to reduce *o*-CNB to *o*-CAN (E (*o*-CNB/*o*-CAN) = -0.4 eV⁷⁹ vs. SHE). Many researches on the photocatalytic redox reactions over semiconductors were focused on the electron transfer between surface-bound species and the CB and the VB of the photocatalyst. Mayer et al. reported that reduced TiO_2 and ZnO nanoparticles in solution could transfer an electron and a proton to phenoxyl and nitroxyl radicals, indicating that e^- and H^+ coupled on the interface. The reduced oxides could transfer both electron and proton, which will expand the traditional view of interfacial redox reactions.⁷⁹ Therefore, *o*-CNB could be reduced to *o*-CAN by the couple of e^- and $\bullet CO_2^-$ with H^+ in the present system, and the reaction proceeded through the hydrogen transfer between *o*-CNB and HCOOH molecules.

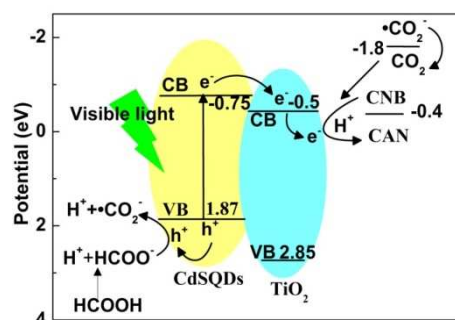


Fig. 10 Proposed mechanisms for the photoreduction of *o*-CNB over CdS QDs-P25.

Conclusions

CdS QDs sensitized P25 (CdS QDs-P25) was prepared by tethering CdS QDs with P25 through thiol, amino and carboxyl group of bifunctional molecular linker of L-cysteine. The absorption band of P25 was extended from the UV region to the visible region after sensitized by CdS QDs. The CdS QDs-P25 showed higher photocatalytic activity in the reduction of *o*-CNB under the visible region (≥ 420 nm) in the presence of sacrificial agent by comparing to P25, CdS QDs and CdS-P25. Based on the results of the characterization and the experimental data, the reasons for the high activity of CdS QDs-P25 are concluded to (1) the interaction between CdS QDs and P25 was much stronger; (2) CdS QDs could provide more photocharges than CdS as the particle size effect; (3) the photocurrent value of CdS QDs-P25 was much higher than that of CdS-P25, and (4) E_{CB} of CdS QDs is more cathodic than that of CdS, resulting in much higher driving forces of electron injection formed in CdS QDs-P25. Under visible-light irradiation, once CdS QDs was excited, the photogenerated electrons transferred from the VB to the CB, and injected into the CB of inactivated TiO_2 . Meanwhile, holes generated in the VB of CdS QDs could oxidize $HCOO^-$ to give $\bullet CO_2^-$ and H^+ . On the other hand, the photogenerated electrons were trapped by Ti^{4+} and coupled with the H^+ to form the active hydrogen (H^*). The formed H^* instantly added to a molecule of *o*-CNB to produce *o*-CAN. Moreover, $\bullet CO_2^-$ has a strong reducing ability, and can also be coupled with the protons to reduce *o*-CNB. Thus, the reaction proceeded through the hydrogen transfer between *o*-CNB and HCOOH molecules via the couple of e^- and $\bullet CO_2^-$ with H^+ .

Acknowledgements

The authors gratefully acknowledge the financial supports from NSFC 21273222, 21202159, and from Jilin province, China 20100562.

Notes and references

- ^a State Key Laboratory of Electroanalytical Chemistry, Changchun Institute of Applied Chemistry, Chinese Academy of Sciences, Changchun 130022, PR China. Fax & Tel.: +86-431-8526-2410; E-mail: zhaofy@ciac.ac.cn; hycyl@ciac.ac.cn
- ^b Laboratory of Green Chemistry and Process, Changchun Institute of Applied Chemistry, Chinese Academy of Sciences, Changchun 130022, PR China
- ^c University of Chinese Academy of Sciences, Beijing 100049, PR China

- 1 G. Palmisano, E. Garcia-Lopez, G. Marci, V. Loddò, S. Yurdakal, V. Augugliaro, L. Palmisano, *Chem. Commun.*, 2010, **46**, 7074.
- 2 N. Zhang, Y. Zhang, M.-Q. Yang, Z.-R. Tang, Y.-J. Xu, *J. Catal.*, 2013, **299**, 210.
- 3 N. Zhang, M.-Q. Yang, Z.-R. Tang, Y.-J. Xu, *J. Catal.*, 2013, **303**, 60.
- 4 H. Lin, L. Li, M. Zhao, X. Huang, X. Chen, G. Li, R. Yu, *J. Am. Chem. Soc.*, 2012, **134**, 8328.
- 5 M. Xing, W. Fang, M. Nasir, Y. Ma, J. Zhang, M. Anpo, *J. Catal.*, 2013, **297**, 236.
- 6 H. Tada, T. Mitsui, T. Kiyonaga, T. Akita, K. Tanaka, *Nat. Mater.*, 2006, **5**, 782.
- 7 T. Peng, X. Zhang, P. Zeng, K. Li, X. Zhang, X. Li, *J. Catal.*, 2013, **303**, 156.
- 8 Q. Gu, J. Long, L. Fan, L. Chen, L. Zhao, H. Lin, X. Wang, *J. Catal.*, 2013, **303**, 141.
- 9 V. Jovic, W.-T. Chena, D. Sun-Waterhouse, M. G. Blackford, H. Idriss, G. I. N. Waterhouse, *J. Catal.*, 2013, **305**, 307.
- 10 M. R. Hoffmann, S. T. Martin, W. Y. Choi, D. W. Bahnemann, *Chem. Rev.*, 1995, **95**, 69.
- 11 J. Ryu, S. H. Lee, D. H. Nam, C. B. Park, *Adv. Mater.*, 2011, **23**, 1883.
- 12 L. Liu, X. Gu, C. Sun, H. Li, Y. Deng, F. Gao, L. Dong, *Nanoscale*, 2012, **4**, 6351.
- 13 S. Obregón, G. Colón, *Appl. Catal. B: Environ.*, 2013, **140-141**, 299.
- 14 Z. L. Zhang, M. Wan, Y. L. Mao, *J. Photochem. Photobiol. A*, 2012, **233**, 15.
- 15 K. Li, B. Chai, T. Peng, J. Mao, L. Zan, *ACS Catal.*, 2013, **3**, 170.
- 16 W. Teng, X. Li, Q. Zhao, G. Chen, *J. Mater. Chem. A*, 2013, **1**, 9060.
- 17 A. Hagfeldt, M. Gratzel, *Chem. Rev.*, 1995, **95**, 49.
- 18 S. Bai, H. Li, Y. Guan, S. Jiang, *Appl. Surf. Sci.*, 2011, **257**, 6406.
- 19 Y. Chen, L. Wang, G. Lu, X. Yao, L. Guo, *J. Mater. Chem.*, 2011, **21**, 5134.
- 20 Y. Huo, X. Yang, J. Zhu, H. Li, *Appl. Catal. B: Environ.*, 2011, **106**, 69.
- 21 H. N. Kim, T. W. Kim, I. Y. Kim, S.-J. Hwang, *Adv. Funct. Mater.*, 2011, **21**, 3111.
- 22 Q. Zhou, M.-L. Fu, B.-L. Yuan, H.-J. Cui, J.-W. Shi, *J. Nanopart. Res.*, 2011, **13**, 6661.
- 23 Y. N. Huo, J. Zhang, X. F. Chen, H. X. Li, *Int. J. Photoenergy*, 2012, **2012**, 1.
- 24 E. A. Kozlova, N. S. Kozhevnikova, S. V. Cherepanova, T. P. Lyubina, E. Y. Gerasimov, V. V. Kaichev, A. V. Vorontsov, S. V. Tsybulya, A. A. Rempel, V. N. Parmon, *J. Photochem. Photobiol. A*, 2012, **250**, 103.
- 25 S. Liu, N. Zhang, Z.-R. Tang, Y.-J. Xu, *ACS Appl. Mater. Interfaces*, 2012, **4**, 6378.
- 26 Z. Liu, Z. Hu, H. Huang, Q. Zhang, T. Zhang, J. Zhai, L. Jiang, *J. Mater. Chem.*, 2012, **22**, 22120.
- 27 Z. Shao, W. Zhu, Z. Li, Q. Yang, G. Wang, *J. Phys. Chem. C*, 2012, **116**, 2438.
- 28 J.-W. Shi, X. Yan, H.-J. Cui, X. Zong, M.-L. Fu, S. Chen, L. Wang, *J. Mol. Catal. A: Chem.*, 2012, **356**, 53.
- 29 Y. Tian, J. Fu, B. Chang, F. Xi, X. Dong, *Mater. Lett.*, 2012, **81**, 95.
- 30 W. Wilson, A. Manivannan, V.R. Subramanian, *Appl. Catal. A: Gen.*, 2012, **441-442**, 1.
- 31 G. Wu, M. Tian, A. Chen, *J. Photochem. Photobiol. A*, 2012, **233**, 65.
- 32 Y. Zhang, Y. Tang, X. Liu, Z. Dong, H. H. Hng, Z. Chen, T. C. Sum, X. Chen, *Small*, 2013, **9**, 996.
- 33 J. S. Jang, W. Li, S. H. Oh, J. S. Lee, *Chem. Phys. Lett.*, 2006, **425**, 278.
- 34 V. M. Daskalaki, M. Antoniadou, G. L. Puma, D. Kondarides, P. Lianos, *Environ. Sci. Technol.*, 2010, **44**, 7200.
- 35 D. R. Larson, W. R. Zipfel, R. M. Williams, S. W. Clark, M. P. Bruchez, F. W. Wise, W. W. Webb, *Science*, 2003, **300**, 1434.
- 36 J. B. Sambur, S. C. Riha, D. Choi, B. A. Parkinson, *Langmuir*, 2010, **26**, 4839.
- 37 J. A. McGuire, J. Joo, J. M. Pietryga, R. D. Schaller, V. I. Klimov, *Acc. Chem. Res.*, 2008, **41**, 1810.
- 38 M. C. Beard, *J. Phys. Chem. Lett.*, 2011, **2**, 1282.
- 39 J. S. Nevins, K. M. Coughlin, D. F. Watson, *ACS Appl. Mater. Interfaces*, 2011, **3**, 4242.
- 40 D. G. Sellers, D. F. Watson, *J. Phys. Chem. C*, 2012, **116**, 19215.
- 41 M. E. Kern, D. F. Watson, *Langmuir*, 2012, **28**, 15598-15605.
- 42 J. T. Margraf, A. Ruland, V. Sgobba, D. M. Guldi, T. Clark, *Langmuir*, 2013, **29**, 2434.
- 43 B. R. Hyun, Y. W. Zhong, A. C. Bartnik, L. Sun, H. D. Abruna, F. W. Wise, J. D. Goodreau, J. R. Matthews, T. M. Leslie, N. F. Borrelli, *ACS Nano*, 2008, **2**, 2206.
- 44 R. S. Dibble, D. F. Watson, *J. Phys. Chem. C*, 2009, **113**, 3139.
- 45 S. Qian, C. Wang, W. Liu, Y. Zhu, W. Yao, X. Lu, *J. Mater. Chem.*, 2011, **21**, 4945.
- 46 S. K. Parayil, J. Baltrusaitis, C. M. Wu, R. T. Koodali, *Int. J. Hydrogen Energy*, 2013, **38**, 2656.
- 47 H. Kominami, S.-i. Iwasaki, T. Maeda, K. Imamura, K. Hashimoto, Y. Kera, B. Ohtani, *Chem. Lett.*, 2009, **38**, 410.
- 48 W. Wu, S. Liang, Y. Chen, L. Shen, H. Zheng, L. Wu, *Catal. Commun.*, 2012, **17**, 39.
- 49 W. Wu, L. Wen, L. Shen, R. Liang, R. Yuan, L. Wu, *Appl. Catal. B: Environ.*, 2013, **130**, 163.
- 50 H. Z. Zhu, Y. M. Lu, F. J. Fan, S. H. Yu, *Nanoscale*, 2013, **5**, 7219.
- 51 S. Liu, Y. J. Xu, *Nanoscale*, 2013, **5**, 9330.
- 52 B. Weng, S. Liu, N. Zhang, Z.-R. Tang, Y.-J. Xu, *J. Catal.*, 2014, **309**, 146.
- 53 X. Liu, D. Sun, R. Yuan, X. Fu, Z. Li, *J. Catal.*, 2013, **304**, 1.
- 54 W. Wu, G. Liu, S. Liang, Y. Chen, L. Shen, H. Zheng, R. Yuan, Y. Hou, L. Wu, *J. Catal.*, 2012, **290**, 13.
- 55 Z. D. Meng, M. M. Peng, L. Zhu, W. C. Oh, F. J. Zhang, *Appl. Catal. B: Environ.*, 2012, **113**, 141.
- 56 H. Zhang, X. Lv, Y. Li, Y. Wang, J. Li, *ACS Nano*, 2010, **4**, 380.
- 57 S. Sakthivel, H. Kisch, *Angew. Chem. Int. Ed.*, 2003, **42**, 4908.
- 58 G. Williams, B. Seger, P. V. Kamat, *ACS Nano*, 2008, **2**, 1487.
- 59 H. Shindo, T. L. Brown, *J. Am. Chem. Soc.*, 1965, **87**, 1904.
- 60 Y. K. Sze, A. R. Dvis, G. A. Neville, *Inorg. Chem.*, 1975, **14**, 1969.
- 61 F. Jalilehvand, V. Mah, B. O. Leung, J. Mink, G. M. Bernard, L. Hajba, *Inorg. Chem. Commun.*, 2009, **48**, 4219.
- 62 K. Nakamoto, Y. Morimoto, A. E. Martell, *J. Am. Chem. Soc.*, 1961, **83**, 4528.
- 63 G. B. Deacon, R. J. Phillips, *Coord. Chem. Rev.*, 1980, **33**, 227.
- 64 P. J. Barrie, A. Gyani, M. Motevalli, P. O'Brien, *Inorg. Chem.*, 1993, **32**, 3862.
- 65 Y. S. Park, A. Dmytruk, I. Dmitruk, A. Kasuya, M. Takeda, N. Ohuchi, Y. Okamoto, N. Kaji, M. Tokeshi, Y. Baba, *ACS Nano*, 2010, **4**, 121.
- 66 R. A. Condrate, K. Nakamoto, *J. Chem. Phys.*, 1965, **42**, 2590.
- 67 H. Zaima, N. Ueyama, H. Adachi, A. Nakamura, *Biopolym.*, 1995, **35**, 319.
- 68 Y. Wang, N. Herron, *J. Phys. Chem.*, 1995, **35**, 319.
- 69 Y. Bessekhouad, D. Robert, J. V. Weber, *J. Photochem. Photobiol. A*, 2004, **163**, 569.
- 70 G. Brieger, T. J. Nestrick, *Chem. Rev.*, 1974, **74**, 567.
- 71 R. A. W. Johnstone, A. H. Wilby, *Chem. Rev.*, 1985, **85**, 129-170.
- 72 R. X. Liu, Y. Wang, H. Y. Cheng, Y. C. Yu, F. Y. Zhao, M. Arai, *J. Mol. Catal. A: Chem.*, 2013, **366**, 315.
- 73 H. Y. Cheng, R. X. Liu, Q. Wang, C. Y. Wu, Y. C. Yu, F. Y. Zhao, *New J. Chem.*, 2012, **36**, 1085.
- 74 H. Wiener, J. Blum, Y. Sasson, *J. Org. Chem.*, 1991, **56**, 4481.
- 75 X. X. Zou, G. D. Li, K. X. Wang, L. Li, J. Su, J. S. Chen, *Chem. Commun.*, 2010, **46**, 2112.
- 76 D. M. Stanbury, *Adv. Inorg. Chem.*, 1989, **33**, 69.
- 77 J. Su, X. X. Zou, G. D. Li, L. Li, J. Zhao, J. S. Chen, *Chem. Commun.*, 2012, **48**, 9032.
- 78 H. G. William, J. L. Ferry, *J. Phys. Chem. B*, 1998, **102**, 2239.
- 79 J. N. Schrauben, R. Hayoun, C. N. Valdez, M. Braten, L. Fridley, J. M. Mayer, *Science*, 2012, **336**, 1298-1301.